Figure 19. Luminescence intensity of $(Lu_{0.9}Ce_{0.01})_3Al_5O_{13}$ as a function of temperature.
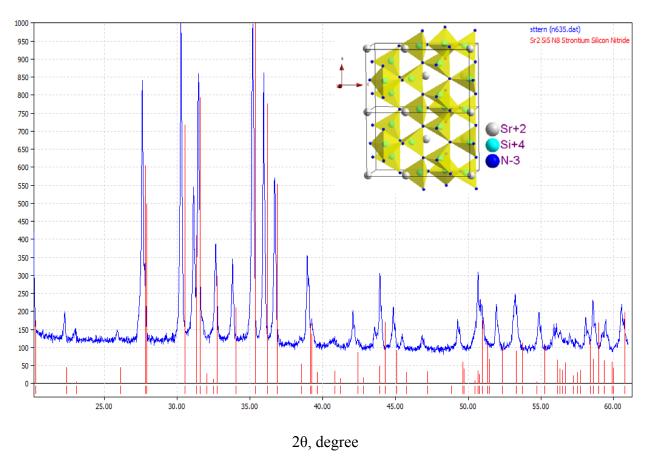

3.3. Red phosphors

In recent years, the research on SiN_4-based covalent nitrides phosphor, including nitridosilicates, nitridoaluminosilicates, sialons, and nitrides *etc.*, for LEDs has received much more attention. This is because the highly condensed SiN_4-based networks and the high strength of the chemical bonding between the constituent elements result in the extraordinary chemical and thermal stability of nitride materials. Furthermore, the high covalent chemical bonding in nitrides and large crystal field effect of nitrogen anion give rise to a strong nephelauxetic effect (*i.e.,* electron cloud expansion), which will reduce the energy of the excited state of the 5d electrons of the activators (e.g., Eu^{2+}, Ce^{3+}) and correspondingly result in larger excitation/emission wavelengths [20–24]. These characteristics make covalent nitrides to be ideal candidates for LED phosphors. Among all candidates for the red phosphors, $M_2Si_5N_8$ (M = Ca, Sr, Ba):Eu^{2+} and $MAlSiN_3$:Eu^{2+} (M = Ca, Sr) were demonstrated to be high promising potential phosphors for InGaN based white-light LEDs.

3.3.1. $(Sr,Ba)_2Si_5N_8$:Eu^{2+}

As for $M_2Si_5N_8$:Eu^{2+} (M = Ca, Sr, Ba), they belong to different crystallographic system [25]. The isostructure of $Sr_2Si_5N_8$ and $Ba_2Si_5N_8$ have an orthorhombic lattice with the space group of $Pmn21$, however, $Ca_2Si_5N_8$ has a monoclinic crystal system with the space group of Cc. The $Eu_2Si_5N_8$ and $M_2Si_5N_8$ (M = Sr, Ba) compounds are also isostructural, therefore, Eu^{2+} ions can be totally incorporated into $Sr_2Si_5N_8$ and $Ba_2Si_5N_8$ forming complete solid solutions. However, Eu^{2+}-doped $Ca_2Si_5N_8$ forms a limited solid solution having a monoclinic lattice. The ideal emission color can be achieved by tuning the nature of M^{2+} and their concentration. We have achieved an optimized composition as $(Sr_{0.82}Ba_{0.15}Eu_{0.03})_2Si_5N_8$, whose XRD pattern is shown in Figure 20. In Figure 20, the red lines denote the standard peaks of $Sr_2Si_5N_8$ (JCPDS: 85-0101) and the blue line is the measured data. All diffraction peaks blueshift with Ba^{2+} co-doped into $Sr_2Si_5N_8$, because the ionic radius of Ba^{2+} is larger than that of Sr^{2+} (Ba^{2+}:1.34; Sr^{2+}:1.12). The $(Sr_{0.82}Ba_{0.15}Eu_{0.03})_2Si_5N_8$ phosphor was

synthesized with high pressure method from the precursors of EuN, Sr_3N_2, Ba_3N_2 and Si_3N_4 in nitrogen atmosphere in our group. The three-dimensional framework structure of $Sr_2Si_5N_8$ is constructed by corner-sharing SiN_4 tetrahedron, as the inset shown in Figure 20, where half the nitrogen atoms are connected to two Si neighbors ($N^{[2]}$) and the other half have three Si neighbors ($N^{[3]}$). There are two M sites in $M_2Si_5N_8$ (M = Sr, Ba) crystal lattice. The $N^{[3]}$ atoms are arranged in corrugated sheets perpendicular to [100]; and the M^{2+} ions, which are mainly coordinated by $N^{[2]}$ atoms (E-N: 2.60–3.25 Å), are situated in channels along [100] formed by Si_6N_6 rings [25–28]. The coordination numbers are 8 and 10 for M_1 and M_2 sites, respectively [25–28]. Thus, there would be a large difference in coordination environment (and thus crystal field) for Eu^{2+} in two different M sites (the mean distance: Sr_1–N = 2.865(6) Å *versus* Sr_2–N = 2.928(7) Å; Ba_1–N = 2.917(3) Å *versus* Ba_2–N = 2.981(5) Å). However, another viewpoint considers that the coordination number are both 10, just only there are two distinct coordination surroundings for Sr^{2+}, one with an average distance of 3.5 Å and the other 2.969 Å [29]. Despite of the significant controversies over this problem, two types of Sr^{2+} site are commonly accepted. As expected, two evident emission bands should be observed for the Eu^{2+} ions occupying two M sites in $Sr_2Si_5N_8$.

Figure 20. XRD pattern of $(Sr_{0.82}Ba_{0.15}Eu_{0.03})_2Si_5N_8$. Inset presents its three-dimensional framework structure.

2θ, degree

The emission (λ_{ex} = 460 nm) and excitation (λ_{em} = 632 nm) spectra of $(Sr_{0.82}Ba_{0.15}Eu_{0.03})_2Si_5N_8$ are shown in Figure 21. The broad emission band peaked at 632 nm is attributed to 5d→4f transition of Eu^{2+}. The strong excitation band in the region of 300–600 nm, which originates from $4f^7$→$4f^65d^1$

transition of Eu^{2+}, matches perfectly for the blue and nUV LEDs. Therefore, $(Sr_{0.82}Ba_{0.15}Eu_{0.03})_2Si_5N_8$ phosphor can down-convert 380–480 nm blue-nUV light from InGaN LEDs into red emission efficiently. After Gaussian deconvolution on an energy scale, the broad emission band in Figure 20 can be well decomposed into two Gaussian components. This phenomenon is more prominent in variable temperature condition.

Figure 21. Emission (λ_{ex} = 460 nm) and excitation (λ_{em} = 632 nm) spectra of $(Sr_{0.82}Ba_{0.15}Eu_{0.03})_2Si_5N_8$.
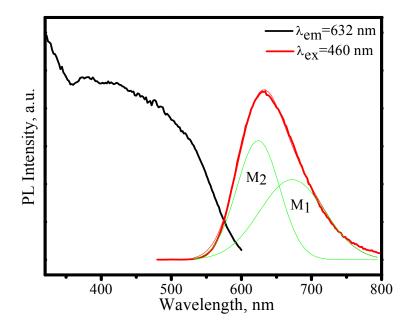

Figure 22 presents the emission spectra of $(Sr_{0.82}Ba_{0.15}Eu_{0.03})_2Si_5N_8$ as a function of temperature, in which the emission peaks blueshit from 632 to 618 nm and the asymmetry of spectral configuration becomes more serious as temperature increases from 25 to 300 °C. Thermal quenching is also observed. As shown in Figure 23, the luminescence intensity of $(Sr_{0.82}Ba_{0.15}Eu_{0.03})_2Si_5N_8$ at 150 and 300 °C are 87% and 34% of its 25 °C value, respectively

As discussed above, there are tow types site of M^{2+} in $M_2Si_5N_8$. Eu^{2+} has the same valence and slightly smaller ionic radius as M^{2+} (Eu^{2+}: 1.09, Sr^{2+}: 1.12, and Ba^{2+}: 1.34). Therefore, from the viewpoint of statistical thermodynamics, it is possible for Eu^{2+} ions to substitute M^{2+} sites randomly in the $M_2Si_5N_8$ crystal lattice. It is well know that the crystal field strength, presented as D_q, is inversely proportional to the 5th power of the bond-length R [30].

$$D_q \propto \frac{1}{R^5} \tag{1}$$

A shorter bond distance implies a stronger crystal field strength. Accordingly, the decrease of the barycenter of excitation band is much higher with nephelauxetic effect and crystal field on the $^4f^65d^1 \rightarrow$ $4f^7$ transition of Eu^{2+} in $M_2Si_5N_8$. Thus, the high-energy emission, as shown in Figure 22, originates from the Eu^{2+} ions which occupy loose crystal circumstance with larger Sr-N bond length (M2); and the low-energy emission originates from the Eu^{2+} ions which occupy compact crystal circumstance with shorter Sr-N bond length (M1). Based on these, the mechanism of the blueshift of emission peaks

with temperature increasing can be explained rationally according to the thermal phonon-assisted tunneling model, as shown in Figure 11.

Figure 22. Emission spectra (λ_{ex} = 460 nm) of $(Sr_{0.82}Ba_{0.15}Eu_{0.03})_2Si_5N_8$ under 460 nm excitation measured at different temperature.
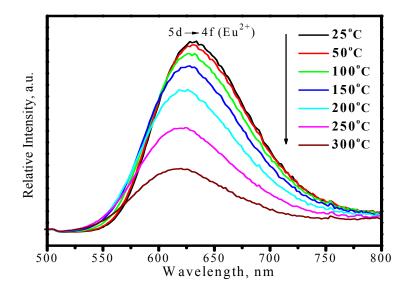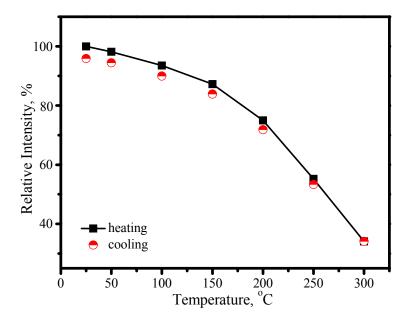

Figure 23. Luminescence intensity of $(Sr_{0.82}Ba_{0.15}Eu_{0.03})_2Si_5N_8$ under 460 nm excitation as a function of temperature.
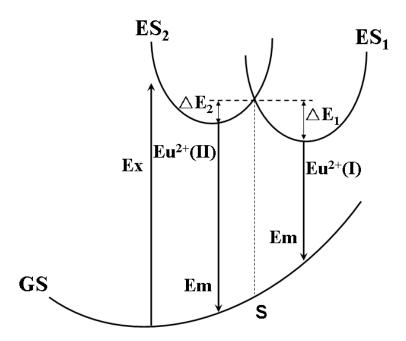

Besides configuration-coordinate model, there is no better physical model to elucidate thermal quenching of luminescence, which is adopted here. As revealed in Figure 24, the thermally active phonon-assisted tunneling from the excited states of low-energy (M_1) emission band to the excited states of high-energy (M_2) emission band in the configuration coordinate diagram increases with an increase of temperature. The energy transfer from the M_1 site to M_2 site through the phonon-assisted tunneling intersection of S point by overcoming the energy barrier and finally reverts to the ground

state to give a shorter wavelength emission. The probability of an electron making the transition via point S is generally described as following relation:

$$\alpha = s \exp(\frac{-\Delta E}{KT})$$ (2)

where K in the formula (1) presents the Boltzmann constant and s is the frequency factor. This transition is strongly dependent on the energy barrier ΔE and temperature T. The probability α generally increases with temperature increasing. Additionally, the 4f electron in the excited state crosses the intersection point between the $4f^6 5d$ and $4f^7$ states of Eu^{2+} ion through thermal phonon-assisted tunneling and returns to the ground state nonradiatively. Therefore, the Eu^{2+} emission peaks blueshift and luminescence intensity decreases with an increase of temperature.

Figure 24. Thermally active phonon-assisted tunneling of Eu^{2+} from low-energy site to high-energy site in configuration-coordinate diagram.

Notes: GS: ground state; ES: excited state; Ex: excitation; Em: emission; S: energy barrier of excited state compared to ground state; ΔE_1 and ΔE_2 denote the energy barrier for the transitions of ES$_1$→ES$_2$ and ES$_2$→ES$_1$, respectively.

3.3.2. (Sr,Ca)SiAlN$_3$:Eu^{2+}

CaAlSiN$_3$ has an orthorhombic structure with space group of Cmc2$_1$ (No. 36) [31–32]. The XRD pattern of (Sr,Ca)SiAlN$_3$ phosphor synthesized in our group is consistent with reference [33], as shown in Figure 25. In accordance with the space group, Al and Si atoms in the crystal distribute randomly at 8b sites. The inset in Figure 25 presents the three-dimensional structure of CaAlSiN$_3$. The tetrahedra of SiN$_4$ and AlN$_4$ form a six-member ring by sharing corner and Ca^{2+} ion locates in the centre of the ring. The rings consisted of the six tetrahedra form a sheet-A by linking together parallel to the a, b-plane. Another sheet B, which is equivalent to the sheet-A rotated by 21 operation, is overlaid on the sheet-A

to form a rigid three dimensional framework. Two-thirds of the N atoms are coordinated with three Si atoms and one-third N atoms are coordinated with two Si atoms. Ca^{2+} ions are accommodated in cavities in the overlaid planes. The Ca site is coordinated with one N atom at a bond length of 0.2490(5) nm, two at about 0.2405(3) nm, one at about 0.2539(5) nm, and another N atom is located at 0.2586(5) nm separation. Therefore, the Ca site is four-coordinated when only the nearest-neighbor ions are taken into account, but more exactly five-coordinated. With Eu^{2+} co-doped into $CaAlSiN_3$, unit cell volume is expanded linearly with Eu^{2+} concentration increasing at least up to 20 mol %, because the radius of Eu^{2+} ion is larger than that of Ca^{2+} (Ca^{2+}:0.99; Eu^{2+}:1.09). Therefore, Eu^{2+} ions should take place of Ca^{2+} sites in crystal lattice. The emission color and intensity of Eu^{2+} depends on Eu^{2+} concentration.
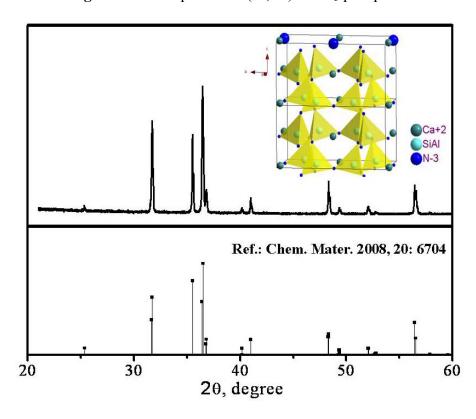
Figure 25. XRD pattern of $(Sr,Ca)SiAlN_3$ phosphor.

According to Uheda's results [32], the emission intensity reaches maxima when Eu^{2+} concentration was 1.6% mol, but the wavelength of emission band with a peak at about 650 nm is too long and even some have been out of visible range. Such red emission is difficulty to mix with other emission color to form a good white light. The emission band is blueshifted by co-doping with proper Sr^{2+} and correspondingly, luminescence intensity is improved. An optimized composition, namely $(Sr_{0.75}Ca_{0.25})_{0.98}SiAlN_3:Eu^{2+}_{0.02}$, has been obtained in our group.

Figure 26 presents the emission spectrum under 460 nm excitation and the excitation of $(Sr_{0.75}Ca_{0.25})_{0.98}SiAlN_3:Eu^{2+}_{0.02}$ by monitoring Eu^{2+} emission at 635 nm. The excitation matches perfectly for the blue and nUV LEDs, which indicates that $(Sr_{0.75}Ca_{0.25})_{0.98}SiAlN_3:Eu^{2+}_{0.02}$ phosphor can down-convert 380–450 nm blue-nUV light from InGaN LEDs into red emission efficiently. The peak of emission bands blueshift from about 635 to 631 nm with an increase of temperature from 25 to

300 °C, as shown in Figure 27. The thermal quenching is also observed. The luminescence intensity at 150 and 300 °C is 87 and 58% that of at 25 °C, respectively, as shown in Figure 28. From Figure 28, we get to know that the thermal quenching is recoverable for the duplicate curve of heating and cooling process. The mechanism of the blueshift of emission bands and the thermal quenching of luminescence are similar to those of $(Sr,Ba)_2Si_5N_8:Eu^{2+}$.

Figure 26. Emission (λ_{ex} = 460 nm) and excitation (λ_{em} = 635 nm) spectra of $(Sr_{0.75}Ca_{0.25})_{0.98}SiAlN_3:Eu^{2+}_{0.02}$.
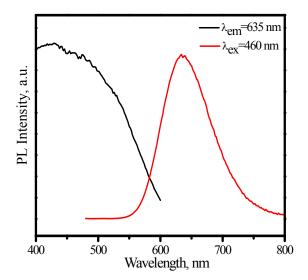

Figure 27. Emission (λ_{ex} = 460 nm) spectra of $(Sr_{0.75}Ca_{0.25})_{0.98}SiAlN_3:Eu^{2+}_{0.02}$ under 460 nm excitation measured at different temperature.
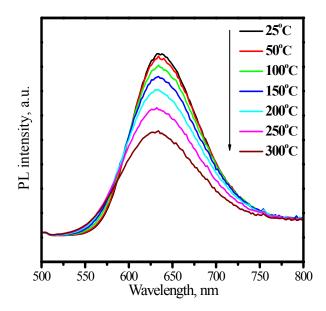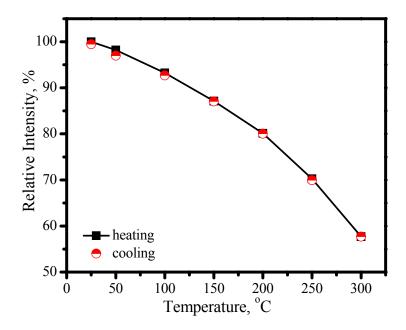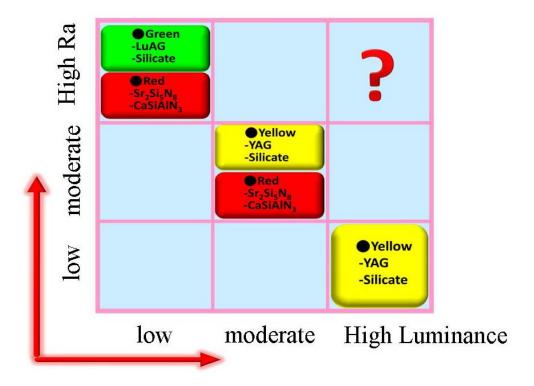
Figure 28. Luminescence intensity of $(Sr_{0.75}Ca_{0.25})_{0.98}SiAlN_3:Eu^{2+}_{0.02}$ under 460 nm excitation as a function of temperature.

4. Conclusions

In conclusion, the strategies for generating white light by combining light-emitting diodes with converting phosphors and the phosphors that are available for producing white light with different luminescence efficiency and color rendering index properties are summarized in this paper. As shown in Figure 1 and Figure 29, to get white light with high efficiency but with low coloring index, yellow phosphors (such as $YAG:Ce^{3+}$ or $(Sr,Ba)SiO_4:Eu^{2+}$) combining with blue LEDs are a good choice, which is suitable for the place that requires high brightness but without high requirement of color rendering; to obtain white light with high color rendering index but with low efficiency, green (such as $LuAG:Ce^{3+}$ or $(Ba,Sr)SiO_4:Eu^{2+}$) and red phosphors (such as $(Sr,Ba)_2Si_5N_8:Eu^{2+}$ or $(Sr,Ca)SiAlN_3:Eu^{2+}$) combining with blue LEDs are a perfect choice, which is suitable for the place that requires high color rendering but without high requirement of efficiency; to achieve white light with appropriate color rendering index and moderate luminescence efficiency, blue LEDs and yellow phosphor (such as $YAG:Ce^{3+}$ or $(Sr,Ba)SiO_4:Eu^{2+}$) by adding proper red phosphors (such as $(Sr,Ba)_2Si_5N_8:Eu^{2+}$ or $(Sr,Ca)SiAlN_3:Eu^{2+}$) are a perfect choice, which is suitable for the circumstance where both the effects of color rendering index and efficiency should be taken into account. Additionally, the white light with high color rendering index and low efficiency can also be produced by combining nUV LEDs with tri-color phosphors, but the luminescence efficiency is very lower comparing with blue LEDs. Up to now, however, the converting phosphors that are convenient to combine with blue LEDs to produce white light with high color rendering index and high luminance have not been found, as the interrogation marked in Figure 29. Therefore, the researches on LED phosphors in future will focus on this point.

Figure 29. Strategies for white light generating by combining blue light-emitting diodes with different converting phosphors.

Acknowledgements

References and Notes

1. Henini, M. The blue laser diode: The complete story (2nd and extended edition): S. Nakamura, S. Pearton, G. Fasol; Springer-Verlag Berlin Heidelberg New York, 368 pages, ISBN: 3-540-66505-6. *Microelectr. J.* **2001**, *32*, 177.
2. Kovac, J.; Peternai, L.; Lengyel, O. Advanced light emitting diodes structures for optoelectronic applications. *Thin Solid Films* **2003**, *433*, 22–26.
3. Nakamura, S.; Senoh, M.; Mukai, T. P-GaN/N-InGaN/N-GaN double-heterostructure blue-light-emitting diodes. *Jpn. J. App. Phys.* **1993**, *32*, L8–L11.
4. Nakamura, S. InGaN-based laser diodes (In Japanese). *Nikkei Electron.* **1994**, *602*, 93.
5. Nakamura, S.; Mukai, T.; Senoh, M. Candela-class high-brightness InGaN/AlGaN double-heterostructure blue-light-emitting diodes. *Appl. Phys. Lett.* **1994**, *64*, 1687–1689.
6. Nakamura, S.; Fasol, G. *The Blue Laser Diode: GaN Based Light Emitters and Lasers*; Springer: Berlin, Germany, 1997; p. 216.

7. Liu, J.; Lian, H.; Sun, J.; Shi, C. Characterization and properties of green emitting $Ca_3SiO_4Cl_2:Eu^{2+}$ powder phosphor for white light-emitting diodes. *Chem. Lett.* **2005**, *34*, 1340–1341.

8. Schubert, E.F.; Kim, J.K. Solid-state light sources getting smart. *Science* **2005**, *308*, 1274–11278.

9. Liu, R.S.; Liu, Y.H.; Bagkar, N.C.; Hu, S.F. Enhanced luminescence of $SrSi_2O_2N_2:Eu^{2+}$ phosphors by codoping with Ce^{3+}, Mn^{2+}, and Dy^{3+} ions. *Appl. Phys. Lett.* **2007**, *91*, 061119.

10. Mancic, L.; Marinkovic, K.; Marinkovic, B.A.; Dramicanin, M.; Milosevic, O. $YAG:Ce^{3+}$ nanostructured particles obtained via spray pyrolysis of polymeric precursor solution. *J. Eur. Ceram. Soc.* **2010**, *30*, 577–582.

11. Li, Y.X.; Min, Y.L.; Zhou, X.Z.; You, X.Z. Coating and stability of YAG:Ce phosphor synthesized using inorganic-organic hybrid gel method. *Chin. J. Inorg. Chem.* **2003**, *19*, 1169–1174.

12. Lu, C.H.; Hong, H.C.; Jaganathan, R. Sol–gel synthesis and photoluminescent properties of cerium-ion doped yttrium aluminium garnet powders. *J. Mater. Chem.* **2002**, *12*, 2525–2530.

13. Zhou, Y.; Lin, J.; Yu, M.; Wang, S.B.; Zhang, H.J. Synthesis-dependent luminescence properties of $Y_3Al_5O_{12}:Re^{3+}$ (Re = Ce, Sm, Tb) phosphors. *Mater. Lett.* **2002**, *56*, 628–636.

14. Shi, S.K.; Wang, J.Y. Combustion synthesis of Eu^{3+} activated $Y_3Al_5O_{12}$ phosphor nanoparticles. *J. Alloys Compounds* **2001**, *327*, 82–86.

15. Larson, A.C.; Von Dreele, R.B. *Generalized Structure Analysis System (GSAS);* Los Alamos National Laboratory Report LAUR 86–748; Los Alamos National Laboratory: Los Alamos, NM, USA, 1994.

16. Chiang, C.C.; Tsai, M.S.; Hon, M.H. Luminescent properties of cerium-activated garnet series phosphor: Structure and temperature effects. *J. Electrochem. Soc.* **2008**, *155*, B517-B520.

17. Jacobs, R.R.; Krupke, W.F.; Weber, M.F. Measurement of excited-state-absorption loss for Ce^{3+} in $Y_3Al_5O_{12}$ and implications for tunable 5d→4f rare-earth lasers. *Appl. Phys. Lett.* **1978**, *33*, 410–412.

18. Dong, Y.; Zhou, G.; Xu, J.; Zhao, G.; Su, F.; Su, L.; Zhang, G.; Zhang, D.; Li, H.; Si, J. Luminescence studies of Ce:YAG using vacuum ultraviolet synchrotron radiation. *Mater. Res. Bull.* **2006**, *41*, 1959–1963.

19. Catti, M.; Gazzoni, G.; Ivaldi, G. Structures of twinned β-Sr_2SiO_4 and of α'-$Sr_{1.9}Ba_{0.1}SiO_4$. *Acta Crystallogr. C* **1983**, *39*, 29–34.

20. Höppe, H.A.; Lutz, H.; Morys, P.; Schnick, W.; Seilmeier, A. Luminescence in Eu^{2+}-doped $Ba_2Si_5N_8$: Fluorescence, thermoluminescence, and upconversion. *J. Phys. Chem. Solids* **2000**, *61*, 2001–2006.

21. van Krevel, J.W.H.; Hintzen, H.T.; Metselaar, R.; Meijerink, A. Long wavelength Ce^{3+} emission in Y–Si–O–N materials. *J. Alloys Compounds* **1998**, *268*, 272–277.

22. van Krevel, J.W.H.; van Rutten, J.W.T.; Mandal, H.; Hintzen, H.T.; Metselaar, R. Luminescence properties of terbium-, cerium-, or europium-doped α-sialon materials. *J. Solid State Chem.* **2002**, *165*, 19–24.

23. Xie, R.J.; Mitomo, M.; Uheda, K.; Xu, F.F.; Akimune, Y. Preparation and luminescence spectra of Calcium- and Rare-Earth (R = Eu, Tb, and Pr)-codoped α-SiAlON ceramics. *J. Am. Ceram. Soc.* **2002**, *85*, 1229–1234.

24. Uheda, K.; Takizawa, H.; Endo, T.; Yamane, H.; Shimada, M.; Wang, C.M.; Mitomo, M. Synthesis and luminescent property of Eu^{3+}-doped $LaSi_3N_5$ phosphor. *J. Lumin.* **2000**, *87–89*, 967–969.

25. Li, Y.Q.; van Steen, J.E.J.; van Krevel, J.W.H.; Botty, G.; Delsing, A.C.A.; DiSalvo, F.J.; de With, G.; Hintzen, H.T. Luminescence properties of red-emitting $M_2Si_5N_8$:Eu^{2+} (M = Ca, Sr, Ba) LED conversion phosphors. *J. Alloys Compd.* **2006**, *417*, 273–279.

26. Huppertz, H.; Schenick, W. $Eu_2Si_5N_8$ and $EuYbSi_4N_7$. The first nitridosilicates with a divalent rare earth metal. *Acta Crystallogr. C* **1997**, *53*, 1751–1753.

27. Duan, C.J.; Otten, W.M.; Delsing, A.C.A.; Hintzen, H.T. Preparation and photoluminescence properties of Mn^{2+}-activated $M_2Si_5N_8$ (M = Ca, Sr, Ba) phosphors. *J. Solid State Chem.* **2008**, *181*, 751–757.

28. Piao, X.; Horikawa, T.; Hanzawa, H.; Machida, K.I. Characterization and luminescence properties of $Sr_2Si_5N_8$:Eu^{2+} phosphor for white light-emitting-diode illumination, *Appl. Phys. Lett.* **2006**, *88*, 161908.

29. Sohn, K.S.; Lee, S.; Xie, R.J.; Hirosaki, N. Time-resolved photoluminescence analysis of two-peak emission behavior in $Sr_2Si_5N_8$:Eu^{2+}. *Appl. Phys. Lett.* **2009**, *95*, 121903.

30. Huang, P.; Cui, C.E; Wang, S. Synthesis and characterization of $Sr_3Al_2O_6$:Eu^{2+}, Dy^{3+} phosphors prepared by sol-gel-combustion processing. *Chin. Phys. B* **2009**, *18*, 4524.

31. Uheda, K.; Hirosaki, N.; Yamamoto, Y.; Naito, A.; Nakajima, T.; Yamamoto, H. Luminescence properties of a red phosphor, $CaAlSiN_3$:Eu^{2+}, for white light-emitting diodes. *Electrochem. Solid-State Lett.* **2006**, *9*, H22–H25.

32. Uheda, K.; Hirosaki, N.; Yamamoto, H. Host lattice materials in the system Ca_3N_2–AlN–Si_3N_4 for white light emitting diode. *Phy. Status Solidi A* **2006**, *203*, 2712–2717.

33. Li, Y.Q.; Hirosaki, N.; Xie, R.J.; Takeda, T.; Mitomo, M. Yellow-orange-emitting $CaAlSiN_3$:Ce^{3+} phosphor: Structure, photoluminescence, and application in white LEDs. *Chem. Mater.* **2008**, *20,* 6704–6714.